Journal of the European Ceramic Society 23 (2003) 839–850

www.elsevier.com/locate/jeurceramsoc

Synthesis and dielectric characteristics of the layered structure $Bi_{4-x}R_xTi_3O_{12}$ (R_x = Pr, Nd, Gd, Dy)

José L. Pineda-Flores[a,*], E. Chavira[a], J. Reyes-Gasga[b], A.M. González[c], A. Huanosta-Tera[a]

[a]*Instituto de Investigaciones en Materiales, Universidad Nacional Autónoma de México, Apartado Postal 70-360, 04510 México, DF, Mexico*
[b]*Instituto de Física, Universidad Nacional Autónoma de México, Apartado Postal 20-364, 01000 México, DF, Mexico*
[c]*EUIT Telecomunicación, Univ. Politécnica de Madrid, Ctra. Valencia km 7, 28031, Madrid, Spain*

Received 3 April 2002; received in revised form 20 June 2002; accepted 30 June 2002

Abstract

Four Aurivillius type systems with generic formula $Bi_{4-x}R_xTi_3O_{12}$, where R_x = Pr, Nd, Gd, and Dy, have been synthesised to investigate the physical effects of R_x on the host lattice $Bi_4Ti_3O_{12}$. Particularly we report here the crystallographic characteristics, as measured by X-ray, and the dielectric properties of the resulting compounds. The layered orthorhombic structures show variations of the a/b distortion comparable with that of $Bi_4Ti_3O_{12}$. Impedance spectroscopy is used to display the electrical response over a wide temperature range, from room temperature up to 850 °C. The conductivity diminishes as the size of R_x grows; activation energies are reported. The rare earth concentration determines the ferroelectric characteristics of the compounds: for small x, they behave as typical ferroelectrics, but all of them tend to become relaxors when x grows. The structure seems to favour the appearance of ferroelectricity when the atomic size of the rare earth diminishes. SEM reveals microscopic composition fluctuations in all samples. Using the specimens as if they were the detectors of the electron microscope, we have determined the type of charge carrier involved in the conductivity phenomena.

Keywords: $Bi_4Ti_3O_{12}$; Dielectric properties; Ferroelectric properties; Layered structures; Relaxors

1. Introduction

Attention to Aurivillius phases, which constitute a wide family of layered compounds, has increased because of their potential use in electrooptic devices. They are generically described as $M_{n+1}B_nO_{3n+1}$, where both M and B are ions with suitable chemical valence and ionic radii, as for example M = Bi^{3+}, Pb^{2+}, Ba^{2+}, Sr^{2+}, Ca^{2+}, Na^+, K^+ or rare-earth elements, B = Ti^{4+}, Nb^{5+}, Ta^{5+}, Fe^{3+}, or Ga^{3+}. Most of the synthesised compounds show ferroelectric properties, many with high transition temperature and reasonable degrees of spontaneous polarisation.[1] It is also accepted that a large number of ferroelectric compounds of the Aurivillius phases are displacive, whose perturbations can be referred to a high symmetry parent structure, I4/mmm, with $a_p = b_p \cong 3.85$ Å, p for perovskite.[2,3]

A series of compositions, $Bi_{4-x}R_xTi_3O_{12}$, where R_x represents a rare earth, has been prepared. These compounds belong to the Aurivillius type, so the structures of interest comprise perovskite-like $M_{n-1}B_nO_{3n+1}$ slabs regularly interleaved with Bi_2O_2 layers, where $n = 1,2,\ldots,5$. Bismuth layered compounds have high fatigue resistance,[4] which make them suitable as candidates to support multiple switching charge cycles to full polarisation, as is required in information storage applications.

It is considered that the prepared phases result from the introduction of R_x in the ferroelectric $Bi_4Ti_3O_{12}$ lattice, with the R_x ions randomly distributed on the Bi sites, which lie at the cube-octahedral sites of the perovskite structure.[5,6] $Bi_4Ti_3O_{12}$, also written[7] $(Bi_2O_2)^{2+}(Bi_2Ti_3O_{10})^{2-}$, has orthorhombic symmetry ($a = 5.448$ Å, $c = 32.815$ Å and $a/b = 1.007$ at 25 °C), with a layer structure of oxygen octahedra; it has a Curie temperature of 675 °C.[8] Based on its electrical-optical behaviour Cummins and Cross[9] claim that the true point symmetry of $Bi_4Ti_3O_{12}$ is m, i.e., monoclinic rather than

* Corresponding author.
E-mail address: jlpinedaac@yahoo.com.mx (J.L. Pineda-Flores).

0955-2219/03/$ - see front matter
PII: S0955-2219(02)00226-1

orthorhombic, with its spontaneous polarisation vector laying on the monoclinic *a–c* plane at an angle of less than 5° from the plane of the crystal sheets. Rae, et al.,[10] have described the structure of $Bi_4Ti_3O_{12}$, at room temperature, as a commensurate modulation of an *Fmmm* parent structure derived from an idealized *I4/mmm structure*. Despite this view, $Bi_4Ti_3O_{12}$ is usually considered[11] to have a polar orthorhombic structure, space group B2cb, with $a = 5.448$, $b = 5.410$, $c = 32.815$ Å. This last view is comparable with that of Subbarao.[8]

In $Bi_4Ti_3O_{12}$ the polarisation component along *a* and *c* axis may be reversed independently through 180°, which means that the optical indicatrix may be rotated in various ways in the *a–c* plane.[12] This characteristic is particularly useful in memory and display devices, and in modulators.[9]

Looking for the possibility to modify such physical properties as the ferroelectric Curie point and/or the conductive characteristics of the host lattice, we selected Pr, Nd, Gd, and Dy for R_x. The choice takes care of cationic radii in such a way that the twelve-coordination requisite is satisfied. In the structure of $Bi_4Ti_3O_{12}$, the replacement of Bi by Pr, Nd, Gd, or Dy preserves the electroneutrality of the system without any additional compensation charge mechanism.

In reviewing dielectric properties of ferroelectric materials, a common procedure is to analyse the electrical response of a well-sintered compound under an ac field. We have used the impedance spectroscopy technique to describe the dielectric behaviour of such sintered samples. An equivalent circuit, which approximately describes the electrical response of the ceramic system, has been proposed.

Four formalisms[13] can be used in this type of search: impedance (Z^*), admittance [$Y^* = (Z^*)^{-1}$], relative permittivity [$\varepsilon^* = (j\omega C_0 Z^*)^{-1}$], and the electric modulus [$M = (\varepsilon^*)^{-1}$]. We have combined these to get the required information.

2. Experimental

2.1. Sample preparation

The synthesis of the studied compounds was performed by using normal solid state reaction of the constituent oxides. The $Bi_{4-x}R_xTi_3O_{12}$ samples were prepared by mixing with acetone, in an agate mortar, Bi_2O_3, TiO_2 (Strem Chemicals 99.99% purity), and the appropriate rare earth oxide (Nd_2O_3, Pr_6O_{11}, Gd_2O_3, Dy_2O_3) 99.9% purity from CERAC.

In terms of *x*, a listing of the prepared compositions is presented in Table 1.

The oxide mixtures were fired at 900 °C for 19 h in Pt covered crucibles. After that, samples were finely milled and refired at 1050 °C for 22 h. Using a Siemens D500 diffractometer with Cu-$K_{\alpha 1}$ radiation, X-ray powder diffraction experiments were carried out at each step. Dehydrated NaCl was added as the internal standard to determine the lattice parameters.

Table 1

R_x	X ($Bi_{4-x}R_xTi_3O_{12}$)				
Pr	0.4	0.8	1.2	1.6	2.0
Nd	0.4	0.8	1.2	1.6	
Gd	0.2	0.4	0.6	0.8	
Dy	0.2	0.4	0.6	0.8	

One of the difficulties with certain ferroelectric materials is a tendency to form pyrochlore-type rather than perovskite-type structures, resulting in lower permittivity values. We have found that the pyrochlore structure is formed around 800 °C, while perovskite-type structures are formed between 1000 and 1100 °C. The appropriate thermal treatment was then adopted to suppress the parasitic pyrochlore phase.

2.2. Dielectric measurements

Powder materials were cold pressed (50 MPa) into pellets of 13 mm in diameter and approximately 1 mm thick; they were sintered at 1000 °C for 19 h in an ambient atmosphere. Pellets were crack-free. Gold blocking electrodes were attached on the opposite faces of the sintered disc-shaped pellets. The resulting sandwich-like structure was connected with gold strips to platinum wires and placed inside a vertical furnace. Experiments were performed in air atmosphere. The ac measurement instrumentation comprises a Hewlett Packard HP4192A impedance analyser controlled by a PC microcomputer. Constant temperature experiments were carried out in a carefully controlled electric furnace from room temperature up to 850 °C. A chromel/alumel thermocouple was placed 5 mm away from the sample in order to obtain an accurate sample temperature. The specimens were maintained for 1h, at least, at each temperature before taking measurements. Routine scans involved a frequency range of 5 Hz to 13 MHz, and 94 measurements distributed over the full experimental frequency range. The applied root mean squared voltage was 1 V in each case. Measurements were made at both rising and falling temperature, with 20–25 °C steps, reduced close to the transition temperature. Results do not show hysteresis. Therefore, we present here only those data for increasing temperatures.

3. Results

3.1. X-ray data and sintering microstructure

Fig. 1a shows the X-ray powder diffraction diagram from the studied compounds at the selected composition

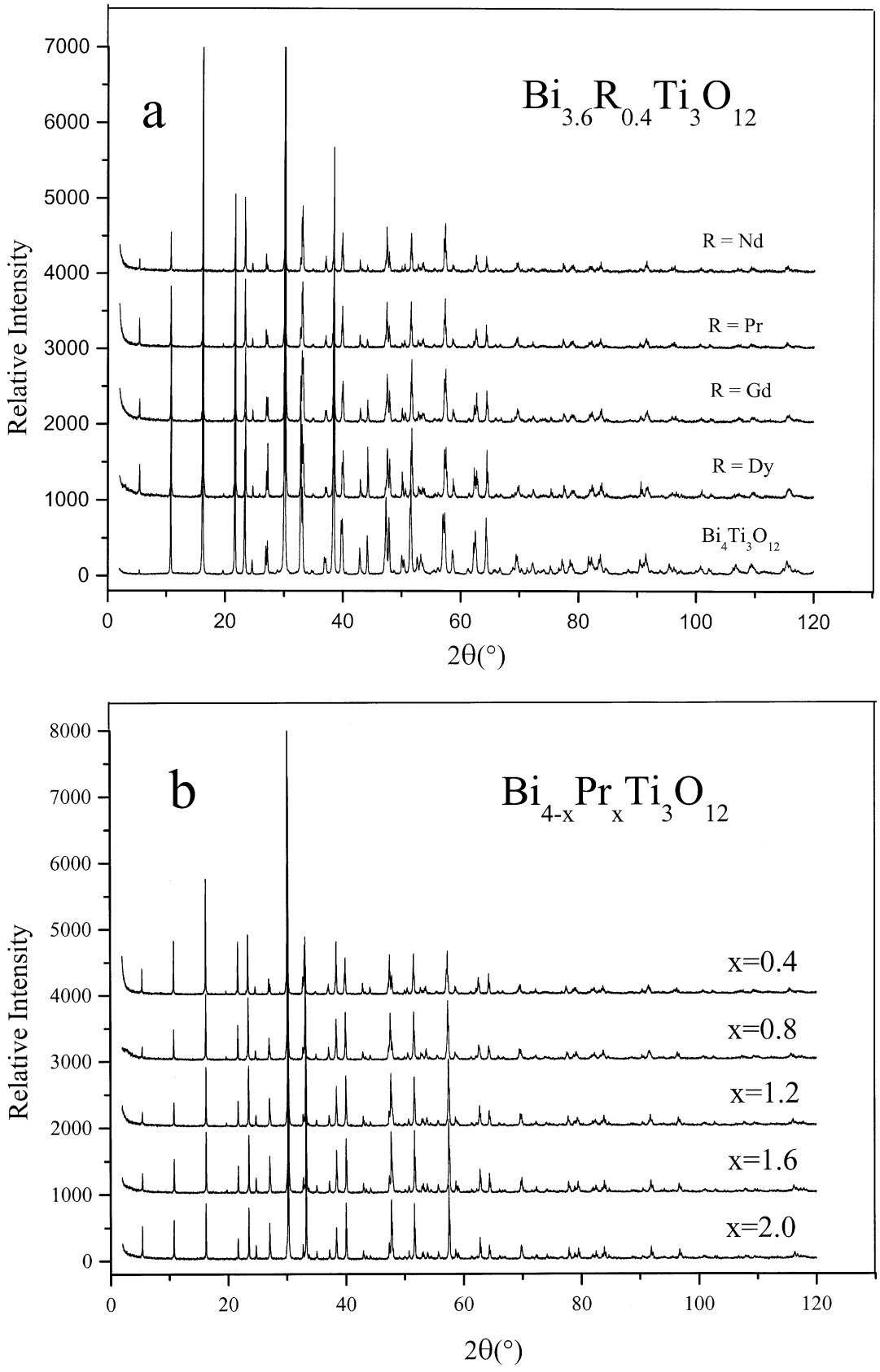

Fig. 1. (a) Powder X-ray diffraction patterns of $Bi_{3.6}R_{0.4}Ti_3O_{12}$ for R = Gd, Nd, Pr, Dy; pattern for $Bi_4Ti_3O_{12}$ is shown as reference; (b) powder X-ray diffraction pattern $Bi_{4-x}Pr_xTi_3O_{12}$ with $x = 0.4$, 0.8, 1.2, 1.6 and 2.0.

$x = 0.4$, in there we have included diffraction data for $Bi_4Ti_3O_{12}$. Fig. 1b exhibits the diffraction characteristics of the solid solution $Bi_{4-x}Pr_xTi_3O_{12}$, for $x = 0.4$, 0.8, 1.2, 1.6, 2.0. Calculus of interplanar spacing corresponding to each peak of X-ray powder patterns was performed automatically, using the DIFRACT-AT V 3.2 program (Socabin-95). As the incorporated rare earth does not modify the scattering of X-ray of the host lattice, the diffraction patterns were indexed on a base-centered orthorhombic structure. All diffraction data processed confirm the existence of an orthorhombic cell. Diffraction patterns were compared particularly with that of $Bi_{3.6}Dy_{0.4}Ti_3O_{12}$, reported in reference.[14] The composition dependence of the lattice parameters is

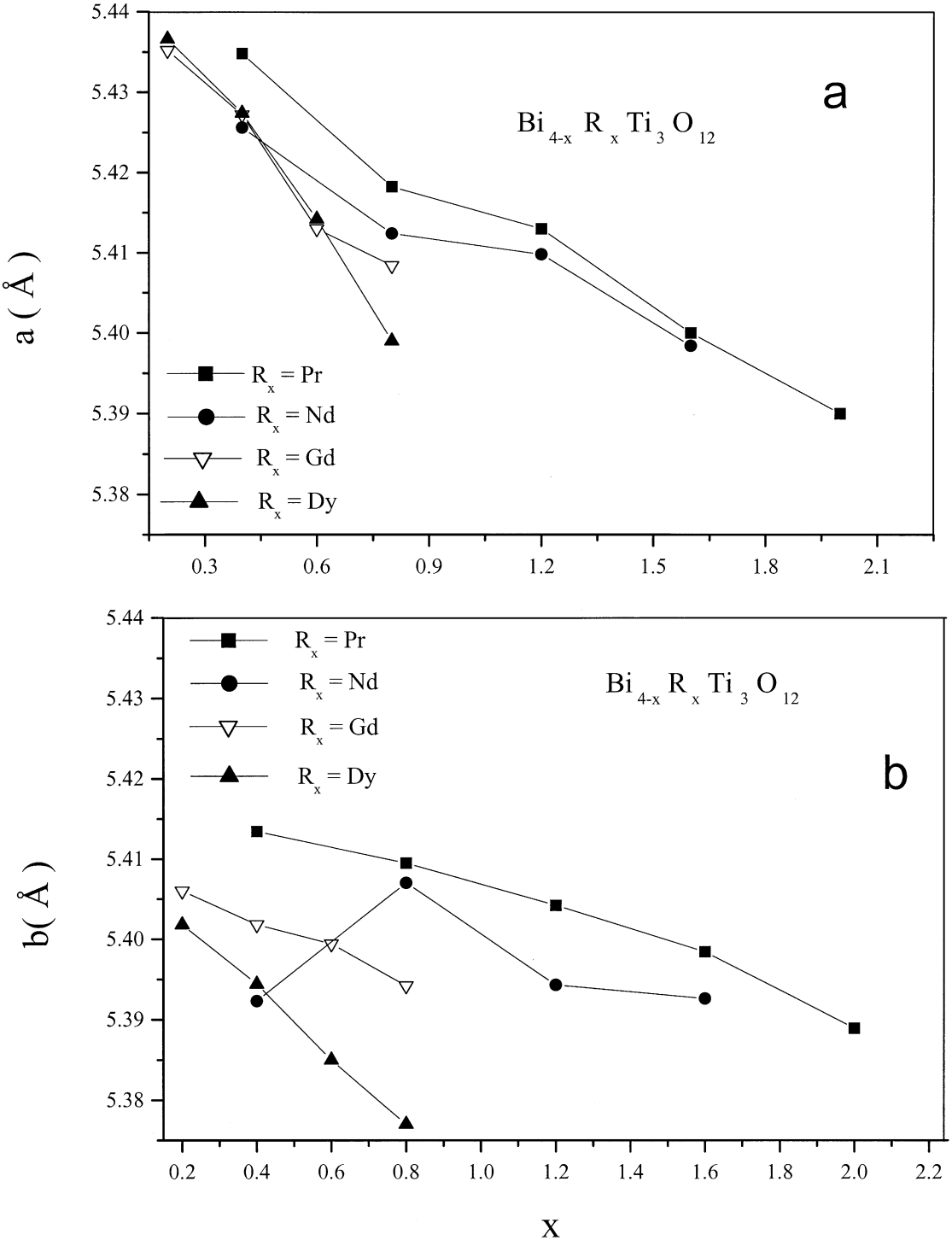

Fig. 2. Lattice parameters of $Bi_{4-x}R_xTi_3O_{12}$ (R_x = Pr, Nd, Gd, Dy) as a function of x: (a) **a** lattice parameter, (b) b lattice parameter, (c) **c** lattice parameter.

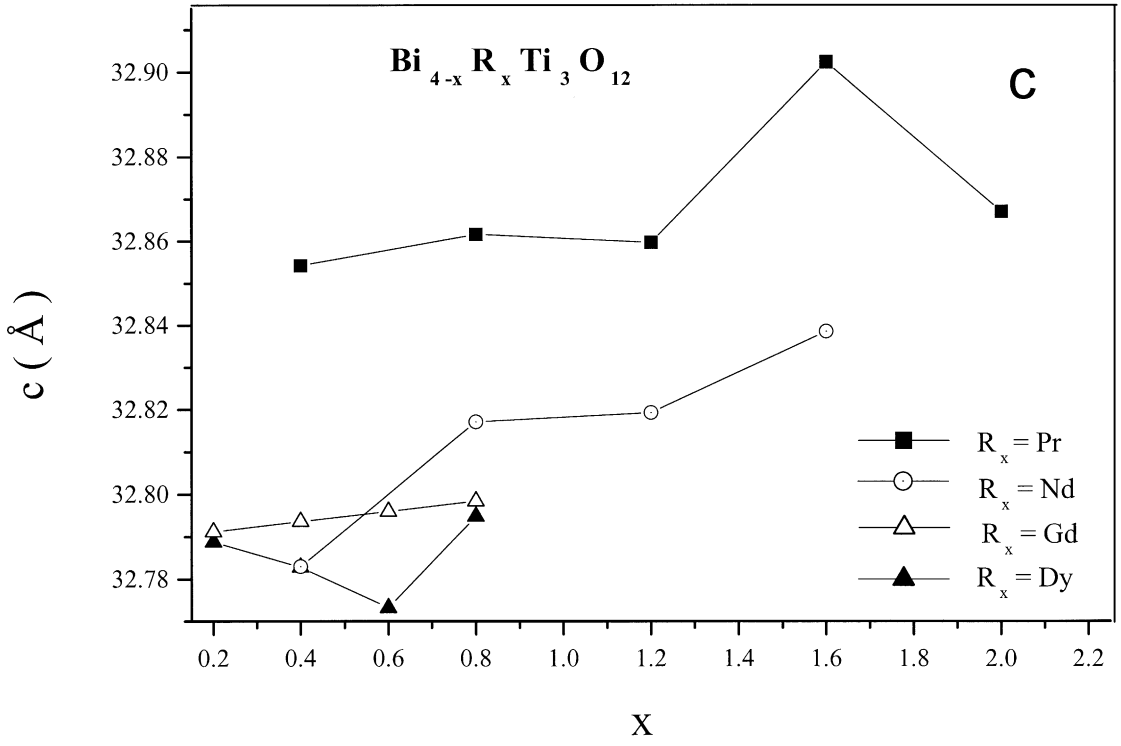

Fig. 2 (*continued*)

presented in Fig. 2a–c. The parameters a and b diminish as x grows. Variation of both a and b keep the orthorhombic distortion, $a/b = 1.007$, very close to that of $Bi_4Ti_3O_{12}$, as given by Subbarao.[8] At the composition $x = 0.8$, for Nd, the b parameter undergoes a sudden and currently unexplained expansion.

Using backscattered and secondary electrons in a scanning electron microscope (Cambridge-Leica Steroescan 440) we have obtained topographical characteristics of fractured samples, a typical microphotograph being shown in Fig. 3, which corresponds to $Bi_{3.6}Nd_{0.4}Ti_3O_{12}$.

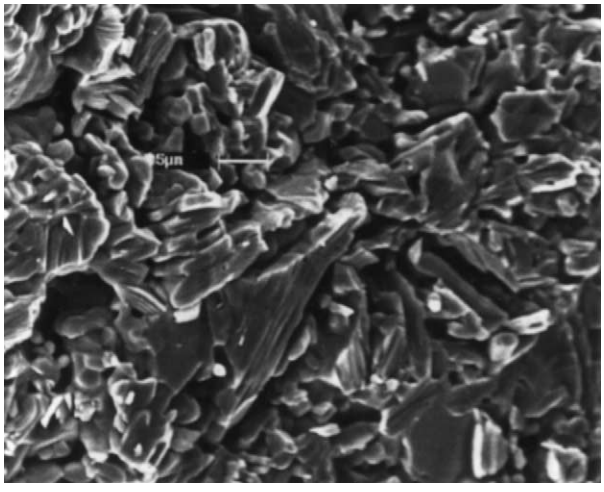

Fig. 3. Secondary electrons microphotograph for a fractured sample of $Bi_{3.6}Nd_{0.4}Ti_3O_{12}$.

From microphotographs we can observe that the densification of the sintered pellets is poor.

We point out that the smaller the × value is, the more inhomogeneous is the resulting grain size distribution. For the smallest x values ($x = 0.2$, 0.4), there are many large grains (~25 μm) and between them, there is a large number of grains exhibiting a wide distribution of smaller sizes (as seen in the secondary electrons microphotograph Fig. 3). When x increases the largest grains tend to disappear and the grain size tend to become homogeneous (~1 μm). An estimate of how the grain size is changing is given by the quotient

$$s_x = \frac{N_x}{N_0},$$

where N_0 is the number of grains per unit area at the smallest x value, and N_x the correspondent number of grains at the different x values. s_x increases more and more while x grows. Consequently the grain boundary density increases.

Electron probe microanalysis was also performed in the electron microscope on polished samples; the results reveal a non-homogeneous rare earth atomic distribution in the analysed regions. Samples were polished mechanically using alumina powder down to 0.05 μm. In large grains, the R_x concentration is depleted towards their edges, while in the smaller grains the composition gradient is difficult to determine. Microanalysis performed at different places randomly chosen over the

samples under analysis did not reveal the presence of the starting materials. The structure of grains in the microphotographs suggested the layered characteristics of the synthesised compounds (Fig. 3).

3.2. Impedance characteristics

There are many reported electrical characterizations of crystalline materials in which the temperature dependence of conductivity is obtained from impedance plots. Therefore, we first analyse the electrical response of the studied samples via impedance curves.

At low temperatures, most of the obtained impedance curves from the four compounds, $Bi_{4-x}R_xTi_3O_{12}$, R_x = Pr, Nd, Gd, and Dy, exhibit a frequency dependent response distributed on two deformed circular arcs.

We present typical impedance curves at selected temperatures for $Bi_{4-x}R_xTi_3O_{12}$ in Fig.4.

Various equivalent circuits were put forward to simulate the experimental response. These are based on the expected physical behaviour within the ferroelectric system and take into account the shape of the individual impedance curves. To start, we suggest an equivalent circuit comprised of two parallel *RC* loops, connected in series. This gives rise to a similar impedance curve as in the experimental case. All *R* and *C* are discrete elements. The used equivalent circuit is also shown in Fig. 4. The impedance is given by $Z^* = [(1/R_1) + j\omega C_1]^{-1} + [(1/R_2) + j\omega C_2]^{-1}$, where $\omega = 2\pi f$ is the angular frequency.

Parameters R_1, R_2, C_1, C_2 were calculated from the impedance curves, both by direct calculation and by using the NLLS-fitting routine by Boukamp.[15] Results for both calculation methods show good agreement.

Next, it is convenient to assign the frequency dispersion data to the physical response of the different regions in the sample. This was discerned by using the impedance representation.

Those arcs at high frequencies have been assigned to the bulk response, because the associated capacitance values (C_1) are in the order of 10^{-12} F. C_1 values were calculated from the maximum condition $2\pi f_{max} RC = 1$, where f_{max} is the frequency associated to the maximum on the arc. The low frequency arc describes grain boundary processes where the capacitance, C_2, has values in the order of 10^{-9} F.[16]

3.3. Grain and grain boundary conductivity

Bulk and grain boundary conductivity, given by $\sigma_b = g/R_1$ and $\sigma_{gb} = g/R_2$, respectively, were plotted in an Arrhenius scheme, where g is a geometrical factor given by the quotient thickness of sample and area of one electrode.

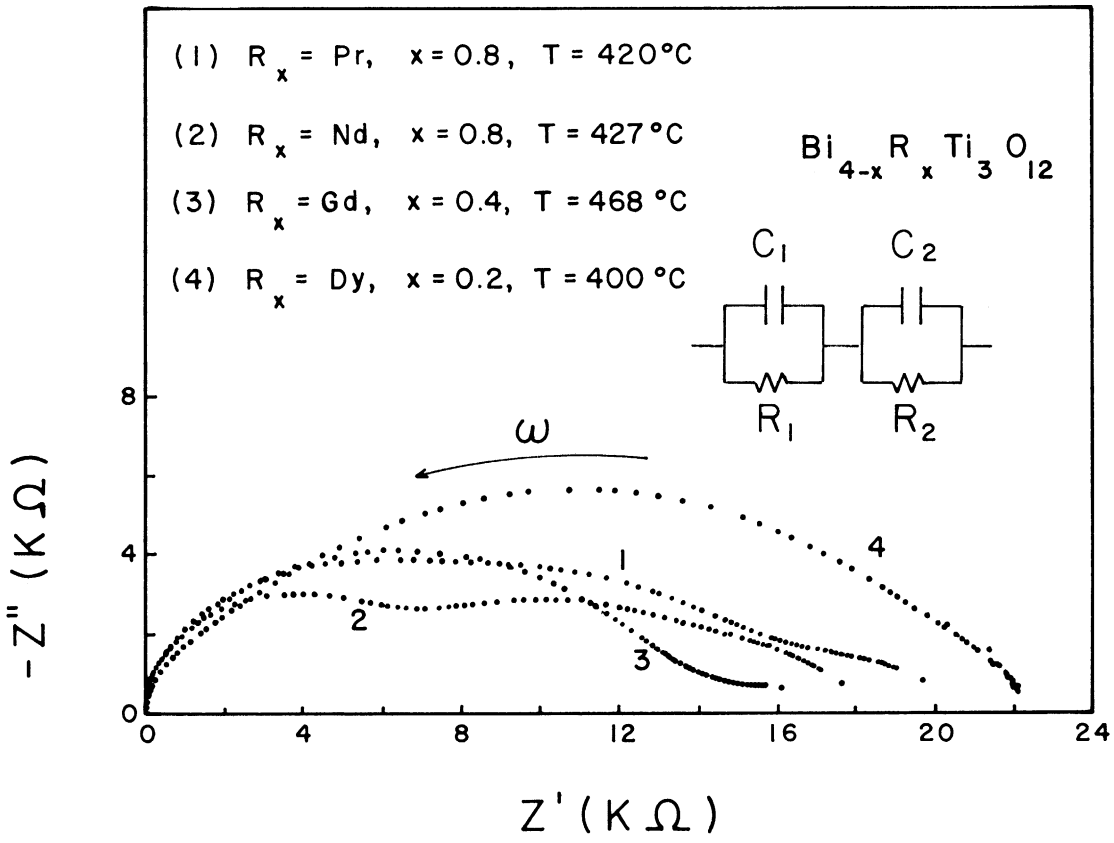

Fig. 4. Typical impedance curves for $Bi_{4-x}R_xTi_3O_{12}$ (R_x = Pr, Nd, Gd and Dy). Curves where chosen for selected temperatures. The equivalent circuit is shown as well.

In general, for each $Bi_{4-x}R_xTi_3O_{12}$, R_x = Pr, Nd, Gd, Dy, studied compound, neither σ_b nor σ_{gb} follows a linear $\log_{10}(\sigma_b, \sigma_{gb})$ vs. 1000/T plot.

In Fig. 5 we have selected the full family of curves for R_x = Pr, to show the typical trend of the bulk conductivity of the four prepared solid solutions; $Bi_{4-x}R_xTi_3O_{12}$. We have included also the temperature dependence of conductivity for the $Bi_4Ti_3O_{12}$ composition; as shown, the host lattice $Bi_4Ti_3O_{12}$ exhibits higher conductivity.

To summarise, the smaller the x-value, the higher the conductivity, for every compound studied. This behaviour may become important to obtain piezoelectric ceramics by means of a polarisation process.

The temperature dependence of the bulk conductivity shows the ferroelectric-paraelectric phase transformation, which was corroborated latter, by exhibiting a slight slope change in the Arrhenius curve. The activation energies (E_a) were determined by fitting each curve $\log_{10}(\sigma_b)$ vs. 1000/T, with the equation $\sigma = \sigma_0 e^{-E_a/kT}$, where k is the Boltzmann constant and σ_0 a pre-exponential factor. The associated activation energies come from two temperature regions, below and above 550 °C. In Table 2 we show all activation energies, described by E_{a1}, and E_{a2} at the low and high temperature intervals, respectively.

We made electron microscope images by charge collection; it was performed through scanning electron microscopy (SEM), whose main characteristic is that the specimen itself is used as the detector. Observations were made on fractured and mechanically polished samples (no chemically attacked) previously tested for conductivity. Electron bombardment of the material will produce an increase of the number of mobile charge carriers, that is because the incident electron beam can transfer enough energy to the sample to promote electrons from the valence band to the conduction band. It

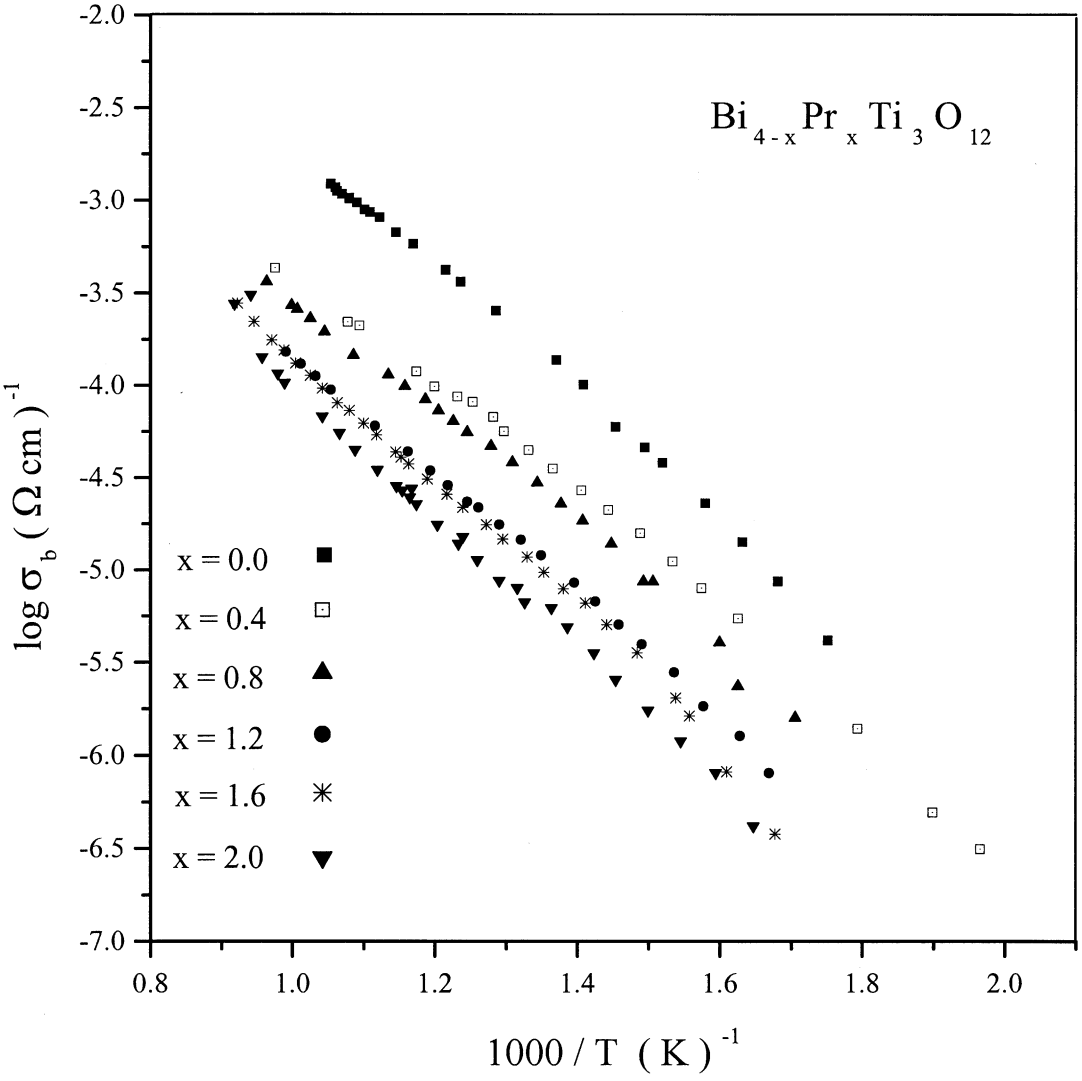

Fig. 5. Arrhenius plot family for $Bi_{4-x}P_xTi_3O_{12}$ (x = 0.4, 0.8, 1.2, 1.6 2.0).

Table 2

$Bi_{4-x}R_xTi_3O_{12}$	E_{a1} (±0.01 eV) T below 550 °C	E_{a2} (±0.01 ev) T above 550 °C	T_c (°C)	ε'_b
R = Nd				
$x=0.4$	0.69	0.55	521	452
$x=0.8$	0.75	0.63	458	390
$x=1.2$	0.75	1.06	395 *	
$x=1.6$	0.76	0.88	340 *	
R = Pr				
$x=0.4$	0.70	0.55	518	566
$x=0.8$	0.66	0.58	482	512
$x=1.2$	0.71	0.62	431 *	
$x=1.6$	0.84	0.75	410 *	
$x=2.0$	0.79	0.71	390 *	
R = Gd				
$x=0.2$	0.87	0.89	618	1503
$x=0.4$	0.76	0.69	584	1162
$x=0.6$	0.68	0.64	514	314
$x=0.8$	0.81	0.81	470 *	
R = Dy				
$x=0.2$	0.72	0.69	604	752
$x=0.4$	0.65	0.81	588	598
$x=0.6$	0.62	0.79	540	428
$x=0.8$	0.60	0.81	462	283

is observed that electrons are more easily generated at small grains, the reason may be that these contain more electrically active defects.

Thus, the obtained images reveal that electronic charge migration occurs mainly through small grains, because the microphotographs show bright contrast in those regions where electrons are present. In contrast, the surfaces of large grains exhibit poor brightness except at the edges. Dark regions are not active in electronic conduction. Using a polished sample, we show in Fig. 6a and b an example of specimen current meter image accompanied by their correspondent backscattering image.

Conductivity through grain boundaries behave as normally occurs in ceramic materials, σ_{gb} is more sensitive than σ_b to temperature changes. In Fig. 7, we show typical variation of σ_b and σ_{gb}, with temperature, for R_x = Nd, with $x=0.8$. The grain boundary resistance seems to have very little effect on the total conductivity.

We propose that the total conductivity can be mainly ascribed to electronic conduction. Electrons are supplied by injection from the electrodes plus a contribution of electrons due to electronic defects. SEM images suggest that particularly small grains in the material supply mobile charge carriers.

3.4. Ferroelectric behaviour

Normally the anomalous behaviour of the temperature dependence of the bulk dielectric permittivity, ε'_b, involves the ferroelectric-paraelectric transition phase exhibiting a maximum value. The condition $\omega_{max}RC=1$ makes C_b virtually frequency independent, so we have obtained the bulk dielectric constant by $\varepsilon'_b = gC_b/\epsilon_0$, where $\varepsilon_0 = 8.854\times10^{-12}$ F/m.

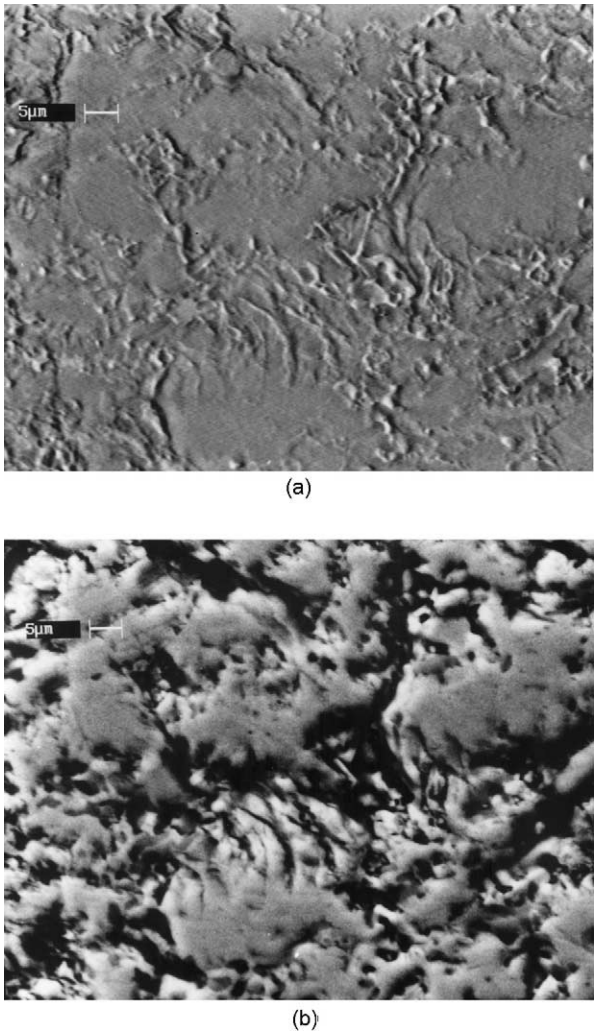

Fig. 6. Scanning electron images on polished samples of $Bi_{3.6}Nd_{0.4}Ti_3O_{12}$ (a) specimen current meter image, (b) backscattering image.

Curves of ε'_b against temperature shows the expected behaviour, as for a normal ferroelectric material, for the prepared $Bi_{4-x}R_xTi_3O_{12}$, with R_x = Gd and Dy, except for $Bi_{3.2}Gd_{0.8}Ti_3O_{12}$ composition. As can be seen in Fig. 8a and b the magnitude of the dielectric constant decreases with increasing R_x concentration. While the rare earth content increases in every studied compound, the Curie point decreases and T_c has values below 675 °C, which corresponds to $Bi_4Ti_3O_{12}$. Observation of Fig. 8a and b, confirms this assertion, T_c falls to 462 °C for $Bi_{4-x}Dy_xTi_3O_{12}$, ($0.2\leqslant x\leqslant 0.8$) and to 514 °C for $Bi_{4-x}Gd_xTi_3O_{12}$ ($0.2\leqslant x\leqslant 0.8$).

Further more, it is evident that in both cases the maximum of ε'_b becomes broader as the ionic radius of R_x grows, making it difficult to determine T_c.

With R_x = Pr, Nd, more serious difficulties arise. In fact, neither of the observed results in the compounds

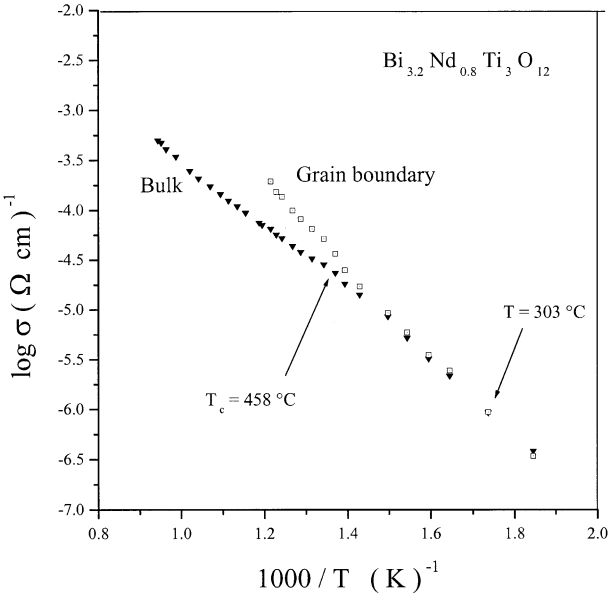

Fig. 7. Typical variation of σ_b and σ_{gb} with temperature for $Bi_{3.2}Nd_{0.8}Ti_3O_{12}$. Two temperatures are shown: $T_c = 458$ °C the ferro-paraelectric transition temperature of the compound; 303 °C points out temperature for which, Arrhenius plot for bulk and grain boundary intersect.

incorporating Pr or Nd, follow normal ferroelectric-paraelectric phase transitions.

In these last cases only those compounds for $x = 0.4$, 0.8, behave with acceptable reliability as to determine T_c. The others produce temperature dependent ε'_b curves which exhibit a quite wide diffuse hill. Table 2 gives the composition dependence of T_c. Attempting to solve this situation, we plotted the real part, $\varepsilon'(\omega)$, of the frequency dependent permittivity, $\varepsilon^*(\omega) = \varepsilon'(\omega) + j\varepsilon''(\omega)$, as a function of temperature.

Using $\varepsilon'(\omega) = (g/\varepsilon_o)\{\omega\ Z''[1 + (Z'/Z'')^2]\}^{-1}$, where Z' and Z'' are the real and imaginary parts of the impedance, we obtained curves of $\varepsilon'(\omega)$ against T at the selected frequencies 1, 10, 100, and 1000 kHz. Curves similar to those shown in Fig. 8a and b were obtained, and T_c values determined whenever possible. Nevertheless, in most cases the calculated transition temperatures have considerable error associated to them, because the peak location depends on frequency. This is a characteristic of relaxor materials. In Fig. 9a and b, we show a couple of examples. Approximate T_c values found through this way were also included in Table 2. They are distinguished by a star.

As is well known, for a normal ferroelectric material at temperatures above the transition point the variation of ε'_b as a function of temperature may obey the Curie–Weiss law $\varepsilon'_b = K/(T - T_0)$, where K is the Curie–Weiss constant, and T_0 is a temperature to be determined. It is known that $T_c > T_0$ for first order transitions. K can be determined by the slope of the curve $(\varepsilon'_b)^{-1}$ against T. All compounds were reviewed but only two of them produce results close to the Curie–Weiss law, namely $Bi_{3.4}Dy_{0.6}Ti_3O_{12}$ and $Bi_{3.8}Dy_{0.2}Ti_3O_{12}$ compositions. Nevertheless, we have to mention that even in these cases calculation of K has associated a considerable error in the correlation factor of the $(\varepsilon'_b)^{-1}$ against T plot. Failure of Curie–Weiss law in relaxor materials has been mentioned before.[17]

3.5. High temperature behaviour

As the temperature rises a third arc appears at the low frequency region on the impedance curves, this is linked with the electrical response from the electrode/sample region. A new parallel $R_{el}C_{el}$ combination should be added in series with the above-proposed equivalent circuit.

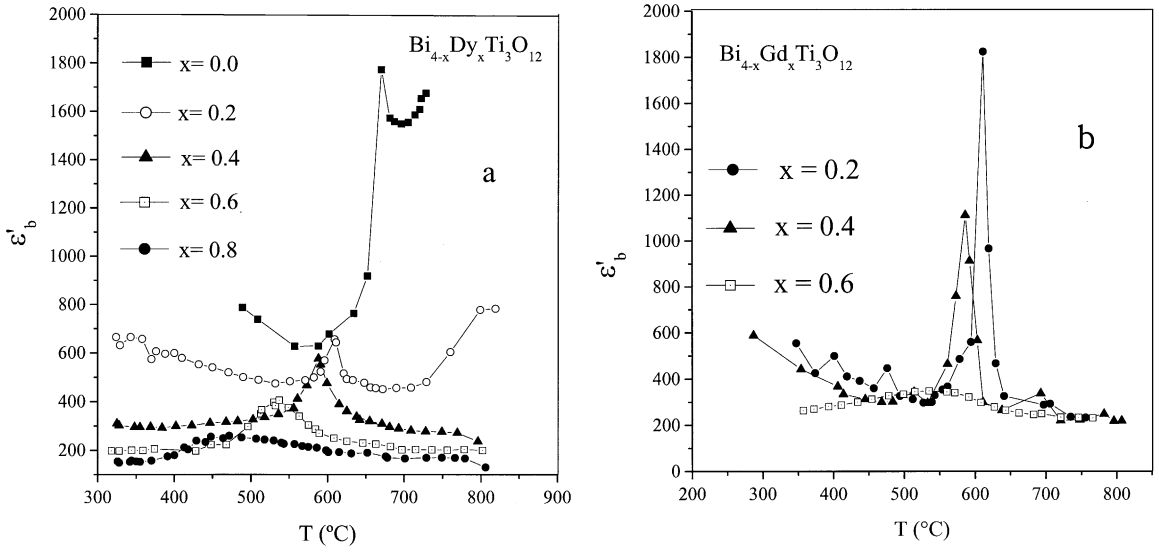

Fig. 8. Dielectric constant versus temperature (a) $Bi_{4-x}Dy_xTi_3O_{12}$, (b) $Bi_{4-x}Gd_xTi_3O_{12}$: $x = 0.2$, 0.4, 0.6, 0.8 in both cases.

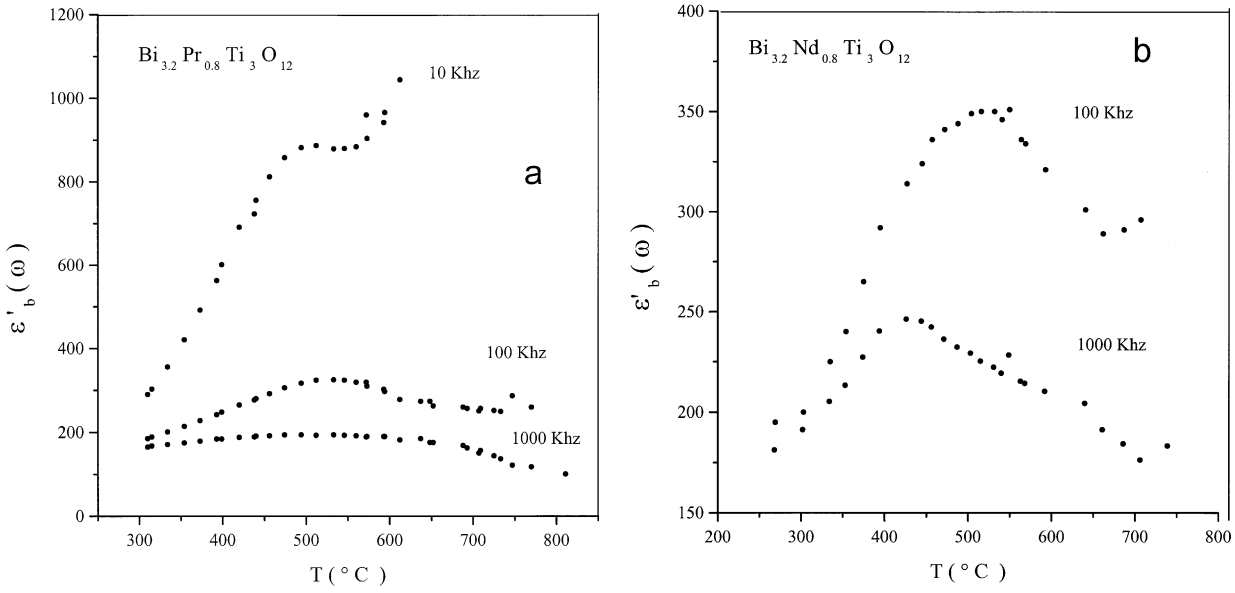

Fig. 9. Real part $\varepsilon'(\omega)$ of the permittivity versus temperature for selected frequencies (a) $Bi_{3.2}Pr_{0.8}Ti_3O_{12}$, (b) $Bi_{3.2}Nd_{0.8}Ti_3O_{12}$.

Calculation of C_{el} ($\cong 1.5$ μF) indicates that effectively the new arc comes from the sample-electrode interface.[11] Probably due to inhomogeneities at the electrode region, R_{el} is a small charge transfer resistance, but it has no special implications in the bulk ferroelectric behaviour.

Finally, at the highest temperatures and most low frequencies, a well-formed spike can be observed, Fig. 10, and a C_d element is added in series with the last circuit. Values in the order of 100 μF for C_d were obtained using the approximation $C_d = 1/(2\pi f Z'')$, Z'' and f being at the spike. Such capacitance values are typical of electrical double layer phenomena, which are characteristic for ionic transport in ceramic materials.[16] However, ionic conductivity has a small contribution to the total conductivity, because at high temperatures there is not a pronounced slope change in the Arrhenius curves, which means that the ionic component does not affect considerably the predominant electronic conductivity.

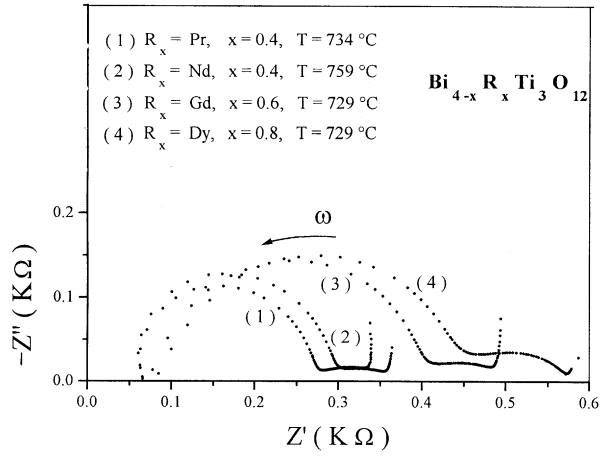

Fig. 10. Impedance curves at temperatures above 550 °C for R_x = Pr, Nd, Gd, Dy. Is shown well-formed spikes.

At this stage impedance curves exhibit a strong deviation at the high frequency region, Fig. 10, a correction given by ωL was used when necessary. L is an inductance associated with the connections between impedance analyser and sample.

4. Discussion

As already mentioned, all of the selected rare earths have atomic number close to that of the Bi atom and the scattering of X-rays is very similar to that one from $Bi_4Ti_3O_{12}$ compound; the prepared samples produce diffraction patterns that correspond to the expected layered phases. All intense reflections show excellent matches with those in the literature. Besides, as in the case of $Bi_4Ti_3O_{12}$ compound, X-ray diffraction from the prepared samples seems to be insensitive to the monoclinic distortion, if it were present. Inclusion of rare earth atoms in the host lattice influence the grain size, which diminish as x grows, increasing the grain boundary density. This combination should be responsible for the decreasing behaviour in conductivity.

There is no clear relationship between E_{a1} and E_{a2}, they are even equal in some cases. It is difficult to say if deviations are in fact due to error calculations. If we assume an almost linear distribution at each individual Arrhenius curve, the activation energies are nearly constant, close to 0.7 eV. Besides, in this approach we can say that the required energy to activate charge carriers is not affected by incorporating the rare earth to the host lattice. That means; the role of the crystalline network may be physically insignificant.

At low temperature, it is hard to believe that rare earth or bismuth ions can migrate throughout the structure, because their mobility is limited by the oxygen octahedral barriers. Then, it is difficult to become ions into charge carriers available to drift when an electric field is applied. However, as mentioned before, at relatively high temperatures an ionic component has been identified by the electrode behaviour. If the frameworks of the oxygen octahedra become oxygen defective, as suggested in references,[18,19] then oxygen ions constitute the best candidates to form the ionic component.

This possibility can be reinforced because the shape of the frequency dependence of conductivity suggests a hoping mechanism, which could be expected for migration of oxygen ions. In Fig. 11, we show the corresponding behaviour at selected temperatures. Unfortunately bulk relaxation frequencies are difficult to determine and activation energy for the impedance relaxation cannot be found.

Every perovskite type ferroelectric, whose permittivity curve, against T, does not present a sharp peak but rather a diffuse hill, pertains to the class of relaxor materials. One of the accepted models to explain that behaviour was proposed by G.A. Smolenskii,[20] which is essentially based on the existence of compositional heterogeneity. The microscopic composition fluctuations induce the existence of polar micro regions in the material,[21,22] which experience switching between a quite wide variety of orientations, and whose consequence is that the spontaneous polarisation is not suddenly lost at T_c.

Presumably the presence of a major amount of rare earth in the host lattice favours largely the existence of polar regions. The polar micro regions are dynamically disordered by thermal motion until temperatures relatively far below and above the transition temperature, and this is why the relaxation spectra broaden in Fig. 8a and b.

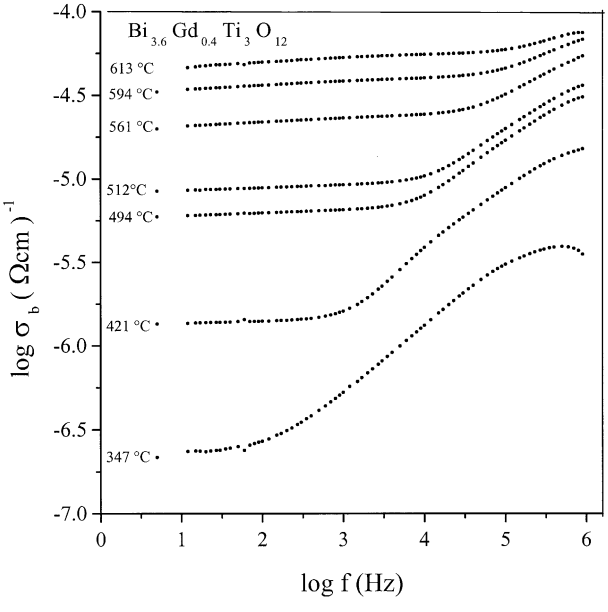

Fig. 11. Conductivity plots for $Bi_{3.6}Gd_{0.4}Ti_3O_{12}$ for several temperatures.

5. Conclusions

Introduction of the rare earth Pr, Nd, Gd, and Dy, in the host lattice $Bi_4Ti_3O_{12}$ produces layered compounds, described by $Bi_{4-x}R_xTi_3O_{12}$, where R_x represents the rare earth, in this work they were synthesised and characterised in its dielectric properties. They are disordered perovskite-type materials. It was found here that the presence of rare earth atoms in the $Bi_4Ti_3O_{12}$ lattice affects its ferroelectric characteristics, changing it to a relaxor. The effect is more important as the concentration of R_x increases and the radii of the rare earth are larger. The occurrence of relaxor behaviour in ferroelectric ceramics is attributable to the presence of compositional heterogeneity in the material. Microscopic compositional fluctuations were detected via microanalysis, performed by electron microscopy techniques. Relatively large differences in composition were localised more frequently on those regions rich in small grain sizes. The bulk ferroelectric-relaxor behaviour was modelled with reliable accuracy by a parallel R_1C_1 loop.

SEM images were used to evaluate conductivity phenomena, as microphotographs exhibit the brightest contrast for small grain sizes, we conclude that they work in conductivity as the principal path of charge carriers.

Evolution of conductivity properties was determined as a function of rare earth concentration. For all cases, conductivity tends to decrease when R_x grows. Electrons are the main charge carriers. Further, the total electronic conductivity was ascribed to a mix of injected electrons from the electrodes plus electrons moving through electronic defects originated by a charge compensation mechanism preferentially located at small particles. They both constitute the dominant factor on the total conductivity.

Appropriate evaluation of dielectric properties was carried out. The maximum of ε'_b becomes broad as the concentration of R_x is increased. Shift of the Curie temperature as a function of frequency observed in $\varepsilon'(\omega)$ versus T plots indicates that most of the studied materials are relaxors ones.

However, more investigation should be made in order to reach a better understanding of the microchemistry and charge transport mechanisms involved.

Acknowledgements

The authors wish thank to Leticia Baños, J. Guzmán M. and Alberto G. Matías Martínez for technical

help. J.L.P. wishes thank to CONACYT the financial support.

References

1. Subbarao, E. C., *J. Am. Ceram. Soc*., 1962, **45**, 166.
2. Withers, R. L., Thompson, J. G. and Rae, A. D., *J. Solid State Chemistry*, 1991, **94**, 404–417.
3. Fritz, B. and Mercurio, J. P., *Journal of Alloys and Compounds*, 1992, **188**, 27–35.
4. Paz de Araujo, C. A., MacMillan, L. D., Cuchiaro, J. D., Scott, M. C. and Scott, J. F., *Nature*, 1995, **374**, 627.
5. Wolfe, R. W. and Newnham, R. E.. *J. Electrochem. Soc. Solid State Science, 1969*.
6. Rentschler, T., Karus, M., Wellm, A. and Reller, A., *Solid State Ionics*, 1996, **90**, 49–55.
7. Subbarao, E. C., *J. Phys. Chem. Solids*, 1962, **23**, 665.
8. Subbarao, E. C., *Physical Review*, 1961, **122**(3), 804.
9. Cummins, S. E. and Cross, L. E., *J. Appl. Phys*., 1968, **39**(5), 2268.
10. Rae, A. D., Thompson, J. G. and Withers, Willis, *Acta Crystallogr*, 1990, **B46**, 474–487.
11. Dorrian, J. F., Newnham, R. E. and Smith, D. K., *Ferroelectrics*, 1971, **3**, 17–27.
12. Barad, Y. and Lettieri, J., *J. Appl. Phys*., 2001, **89**(2).
13. Hodge, I. M., Ingram, M. D. and West, A. R., *J. Electroanal. Chem*., 1976, **74**, 125.
14. Nat. Bur. Stand. (US) Monog. 1984, 25, 2139.
15. Bernard A. Buokamp, ''Equivalent Circuit (equiver.pas)'', University of Twente Dept. Chemical Technology, Netherlands, 1988.
16. Irvine, J. T. S., Sinclair, D. C. and West, A. R., *Adv. Mater*., 1990, **2**, 132.
17. Smolenskii, G. A., *Ferroelectrics*, 1984, **53**, 129–135.
18. Shulman, H. S. and Testof, M., *J. Am. Ceram. Soc*., 1996, **79**(12), 3124–3128.
19. Villegas, M., Moure, C. and Fernández, J. F., *Bol. Soc. Esp. Ceram. Vidr*., 1995, **34**(5–6), 316–321.
20. Smolenskii, G. A., *J. Phys. Soc. of Japan*, 1970, **28**(Suppl.), 26–30.
21. Eric Cross, L., *Ferroelectrics*, 1987, **76**, 241.
22. Kim, Tae-Yong and Jang, Hyun M., *Appl. Phys. Lett*., 2000, **77**(23).